An Experimental Investigation Of The Seismic Behavior Of Brick Walls Reinforced With Hybrid Steel-Glass Fiber Concrete

Elham Bloukyazdi [1], Mohammad Reza Javaheritafti [2]*, Alireza Mirjalili [3]

[1] Ph.D student, Department of Civil Engineering, T.C., Islamic Azad University, Taft, Iran
e.bloukyazdi@iau.ac.ir
[2] Assistant Professor, Department of Civil Engineering, Y.C., Islamic Azad University, Yazd, Iran
MR.Javaheritafti@iau.ac.ir
[3] Assistant Professor, Department of Civil Engineering, Y.C., Islamic Azad University, Yazd, Iran
Alireza.mirjalili@iau.ac.ir
*Corresponding Author: Mohammad Reza Javaheritafti Email: MR.Javaheritafti@iau.ac.ir

Abstract
The existing masonry walls are highly vulnerable to earthquakes. One of the new methods of seismic improvement of existing buildings is the use of concrete coating. This study investigated the effectiveness of enhancing unreinforced masonry (URM) walls using hybrid concrete coating (concrete with steel-glass fibers). This study was experimental and tested two sample walls on a real scale and under an in-plane cyclic loading. One sample was a reinforced wall coated with hybrid fiber concrete (HFC) on one side, and the other was a reinforced wall coated on both sides; meanwhile, an unreinforced wall served as the reference wall. The results revealed that enhancing URM walls with HFC coating provides economic benefits and work simplicity, and most importantly, avoids crack formation by creating a hardened panel. Besides, an HFC layer could considerably enhance the wall's lateral bearing capacity, energy, and stiffness.

Keywords: Hybrid fiber concrete (HFC), Cyclic test, Masonry walls, URM, Steel fiber, Glass fiber, Retrofitted Masonry Brick Walls, Reinforced concrete, Experimental test, Shotcrete.

1. Introduction

Unreinforced masonry (URM) buildings are among the oldest and most common structural types that are highly vulnerable in earthquakes. A number of these buildings have a long history and feature considerable historical value, while some others are important buildings for their special educational roles. There are lots of brick-and-mortar buildings in Iran, many of which are currently facing problems withstanding seismic forces and suffering from structural issues. These buildings are not designed to withstand lateral seismic loads [1]. Concerning the multitude of URM buildings and constructions and their social and economic impacts, reconstruction is not the best solution. Research has broadly investigated the behavior of these types of buildings [2,3,4], indicating the urgent need for evaluating and enhancing the seismic behavior of URM buildings. Studies have mainly examined the reinforcing of the walls as a way to enhance the seismic behavior of these buildings. Overall, the seismic behavior of URM walls can be studied from two in-plane and out-of-plane perspectives. Therefore, enhancing the seismic behavior of walls can be performed according to these two ways.

A body of experimental and numerical research has covered the methods employed to reinforce URM walls, including the use of the concrete face of fiber-reinforced polymer (FRP) plates and prestressing brick walls [5-8]. It is worth mentioning that the materials, implementation methods, and technologies of the construction sector vary from one country to another, and thus we must not merely rely only on the results of studies conducted in other countries. As stated in FEMA356 [9], a strategy to enhance the seismic behavior of URM buildings is to use concrete faces of various types, including concrete reinforced with steel grids and cement-sand mortar-based concrete reinforced with all kinds of fibers. This strategy helps increase the wall's lateral load-bearing capacity and strength, and makes the wall function coherently. Fiber concrete or hybrid fiber concrete (i.e., concretes integrated with two or more fibers) has recently become popular in constructing and retrofitting structural components. This type of concrete is mainly characterized by a greater tensile strength and ductile behavior under tension, which are superior features to conventional concrete. These features are more noticeable in fiber concrete with steel fibers.

Unlike conventional concrete that features a brittle behavior and loses its resistance instantly after reaching the ultimate tensile strength, fiber concrete has its stress-strain curve under tension reduced at a milder slope after reaching the ultimate tensile strength, while reaching the ultimate strain capacity [10]. Besides the basic materials

required to make conventional concrete, fiber concrete is composed of various fibers such as polypropylene fibers, steel fibers, and glass fibers (alone or in combination). These fibers are employed in various dimensions, variable shapes, and different percentages per a specific volume of concrete. The use of HFC is currently a subject of interest for researchers thanks to the positive interaction of fibers, and thereby the enhanced performance of this concrete than fiber concrete containing one type of fiber.

2. Literature review

Zhu et al. studied the properties of fiber concrete and HFC and found that a proper mix design for a hybrid mixture can yield positive fiber interaction, and consequently enhance the concrete's performance [11]. Banthia and Shah studied an HFC made up of two groups of fibers (i.e., with the same type but different sizes) and reported that smaller fibers bridge between small cracks and control the growth of microcracks, thereby preventing them from joining each other. Similarly, they found that larger fibers prevent the creation and development of large cracks [12, 13]. Kwan et al. investigated the properties of HFC and reported that one type of fiber enhances the properties of fresh concrete (e.g., easier production and plastic shrinkage reduction), while the other type enhances the concrete's mechanical properties [14].

Dordai et al. experimentally investigated the seismic behavior of masonry walls enclosed with coils and retrofitted with concrete face reinforced with steel and polypropylene fibers. According to the results, the stiffness and shear strength of the wall reinforced with steel fibers were found to be higher than those in the wall reinforced with polypropylene fibers. Moreover, the fiber-reinforced wall exhibited an 87 to 98% increase in resistance compared to the URM wall [15]. In a 2016 study, Najafgholipour et al. investigated wall prisms retrofitted with steel and polymer mortar faces and found that steel fibers outperformed polymer fibers [15,16,17].

Najafgholipour et al. compared the in-plane behavior of URM panels reinforced with fiber concrete face with sample concrete reinforced with steel grids and found that retrofitting by both methods significantly increased the stiffness and in-plane resistance of all types of masonry walls. Furthermore, enhancing the wall by concrete face reinforced with steel grids, as compared to the concrete face reinforced with fibers, resulted in smaller increases in the wall's resistance, but caused more drift capacity [19].

Yugandhar et al. (2017) studied an HFC made up of a combination of steel and glass fibers with different percentages and reported that combining steel and glass fibers in concrete increased the seismic resistance, life, ultimate load capacity, and stiffness of concrete. Although the resistance parameters will be a bit lower by increasing the percentage of glass fibers in concrete compared to concrete with steel fibers, adding glass fibers enhances ductility and prevents the formation of cracks, while reducing their widths [20].

Sreekrishna et al. studied the use of hooked-end steel fibers of varying lengths in concrete and their impact on the resistance parameters of fiber concrete. The results indicated that using these fibers can enhance the compressive strength, flexural, and tensile strength of concrete. Furthermore, the concrete's durability and mechanical properties were enhanced due to the reciprocal effect of short and long steel fibers. In their study, the fibers had a diameter of 1 mm and lengths of 30 and 60 mm [21]. Guan Li et al. studied the strengthening of six masonry walls using one-sided and two-sided coating methods with HFMRPC fibers. They found that strengthening these walls enhanced the ductility coefficient by 86 to 229% and improved the cumulative energy dissipation by 57 to 139% [22].

In their experimental study, Seyed Rezaei and Soltani investigated the method of retrofitting URM walls using the shotcrete method. The full-scale experiments were performed on six clay walls with cement-and-sand mortar, with the retrofitted samples, experiencing significant increases in lateral strength and cyclic dissipated energy [23].

Babar Ali et al. did some experiments on concrete reinforced with hooked steel, glass, and polypropylene fibers by using a 0.5 and 1.0% v/v combination and evaluated the environmental and economic performance of the designed pavements. The results obtained from mechanical tests revealed that the fiber concrete outperformed the conventional concrete. They concluded that the concrete prepared with the right volume percentages could produce cheaper pavements, while being more compatible with the environment [24].

2. Materials and Methods

2.1. Tested sample Specifications

A two-story URM building was considered as the target building, which well represented URM buildings in Iran. The wall of the building's first story with a 5 m load-bearing span was selected as the test sample. Some specifications of the samples were assumed to be constant in order to correspond to the real conditions of existing buildings in Iran. To this aim, the thickness and height of the walls were considered to be 0.35 and 2.8 m, respectively. Assuming a gravity load of 7 kN/m^2 for each story, the load applied to the wall will be 70 kN/m, which will be on top of the samples' weight. Under this state, the study sample will be subject to a stress of 0.25 MPa at the base level.

The wall's height-to-length ratio was so considered to yield the lateral strength in a way it would allow for the occurrence of the failure mode pertaining to the in-plane deformation. Concerning the type of wall failures (i.e.,

rocking failure), URM walls were selected to compare resistances and achieve an acceptable amount of lateral strength (Q value). Equations to determine capacity for all four failure modes are given in AISC 360 (AISC 360 and ASCE41-17 standard ASCE41-17). In this state, the failure modes of toe pressure and diagonal tension were assumed to be controlled by force, while the failure modes of rocking motion and shear slip of mortar by deformation. Notably, all the instructions (i.e., AISC 360 and standard ASCE41-17). According to the dimensions and characteristics of the investigated wall, the failure mode of the wall is of the cradle type and its relationships are presented in Table 1.

Table 1: Equations related to the wall's capacity after activating rocking failure modes in URM walls

Rocking Failure Mode	
ASCE41-17	Q_{CE}= Vr = 0.9 ($\alpha P_D + \alpha P_w$) (L/heff)
Code 360 (FEMA356)	Q_{CE}= Vr = 0.9 α P_E (L/heff)

Where:
"Vr": The wall's resistance based on the rocking failure mode
"α": A coefficient of 0.5 for the clamped cantilever wall and 1 for the fixed-end wall)
"PD": Axial compressive force caused by a dead load on top of the wall (not considering the effect of the wall's weight)
"L": The wall's length
"heff": The wall's effective height
"PE": Axial compressive force caused by factored gravity loads
Accordingly, a wall of 1.5 m long, which represented no-opening walls, was selected for activating the rocking failure mode. For calculations at this stage, the specifications of high-quality materials were used hypothetically [25, 26]. According to the tests performed on the masonry unit in Figure (1), the lower limit of the shear strength of the mortar Vtl equal to 0.2 MPa and the lower limit of the compressive strength of the wall f'm equal to 4 MPa was determined.

Figure 1: Tests for determining material specifications

After conducting the tests to determine the specifications of the materials (Figure 1), the calculations were repeated based on the actual specifications of the materials, and the results were compared with the experimental results (Table 2).

Table 2: Specifications of the materials

Sample Type	No. of Samples	Reference	Test Description	(Mpa)
Brick	6	ASTM C-67-00 (2002)	Compressive strength	17.8
Load beam & foundation	6	ASTM C39/C39M-99 (2000)	Compressive strength of concrete	28
	3	INSO 3132 (2013)	Yield tensile strength of steel bar T10	560
	3		Yield tensile strength of steel bar T12	540
			Yield tensile strength of steel bar T14	520
Walls mortar	6	ASTM C109/C109M-160 (2016)	Compressive strength	17.3
Masonry units	5	ASTM C-1314-02a (2002)	Compressive strength of masonry units	4.2
	3	ASTM E519-02 (2002)	Tensile strength (diagonal test)	0.4
			Modulus of rigidity	890
	5	ASTM C952-02 (2002)	Bond strength of mortar to masonry units	0.1
			Bed joint shear strength	0.21
	5	Harris and Sabnis (1999)	Coefficient of internal friction (k)	0.51
Shotcrete overlay	3	ASTM C39/C39M-99 (2000)	Compressive strength of hybrid concrete	27

The experimental study was carried out on three sample walls under real conditions. The one- and two-side retrofitting of the wall was performed by the hybrid fiber concrete (HFC) as the main indicator of the study. For this, the walls were constructed with fully similar geometries, which were as much identical as the walls in the Iranian masonry buildings, in terms of bricklaying and materials used (Figure 2).

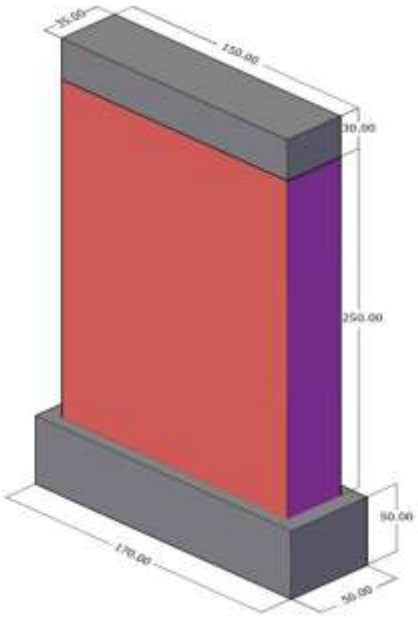

Figure 2: Geometric specifications of the experimental samples

The samples were named UW (control sample), RW_1 and RW_2.
UW: Non-retrofitted unreinforced masonry wall
RW_1: One-side-retrofitted unreinforced masonry wall
RW_2: Two-side-retrofitted unreinforced masonry wall

2.3. Sample Fabrication Procedure

Brick walls were constructed on a reinforced foundation, connected to an experimental rigid plate. To apply a lateral and gravity load to the sample, a reinforced concrete beam was established on the upper part of the wall, which is hereinafter called the loading beam. This will allow for the distribution of loads applied to the wall. Two steel plates are embedded at the two ends of the loading beam (Figure 3).

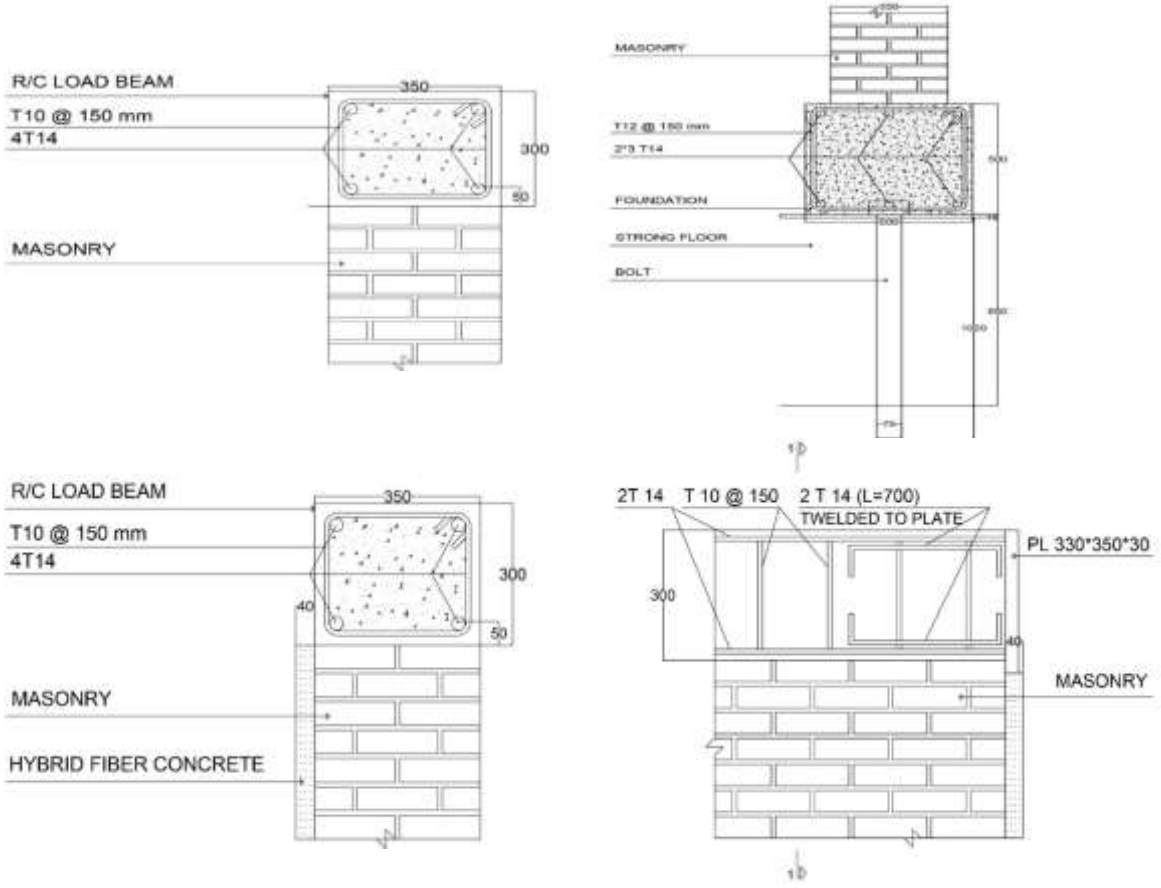

Figure 3: Description of loading reinforced concrete beam

3.3. Materials' Specifications

Masonry walls were constructed by clay pressure bricks whose nominal dimensions featured 220, 110 and 55 mm in length, width, and height, respectively. Bricklaying was performed by using a mortar composed of Portland cement and aggregates of a 1:5 ratio and a water-to-cement ratio of 0.5 [27].
Bricks of similar resistances were used for bricklaying. The slits between the bricks were 10 mm thick. Vertical slits were not filled with mortar in order to make the quality of the walls more similar to the existing masonry buildings across Iran; also the bricks were laid by a professional mason. After the bricklaying and taking care of moisture for 28 days, the wall was reinforced with a face of hybrid fiber concrete (cement-sand mortar and steel-glass fibers) [28].
The cement-sand mortar was made up of a Portland cement-to-aggregates ratio of 1:5, a water-to-cement ratio of 1:2, and fibers with 1% of the total weight of the concrete. The measurements also considered a steel-to-glass ratio of 1:3 [19], with the face thickness considered 40 mm [29].

3.4. Fibers used

Glass fibers

Glass fibers are made of very thin strands of glass type with a fixed constant of around 7-25 μ and an unspecific length, which are considered the most economic types of concrete fibers. The use of these fibers in concrete can affect the reduction of fresh concrete efficiency; for this, appropriate lubricants should be used.

Table 3: Glass fiber specifications

Product Name	Fiber Type	Fiber strength (MPa)	Fiber stiffness (GPa)	Areal weight (g/m^2)	Fabric thickness (mm)	Style	Collapse strain (%)	Texture pattern	Density (gr/m^2)
YC-G420	E-glass	2200	70	400	0.3	Woven UD	2.1	One-directional	2.55

These fibers help create more durability in concrete and increase flexural and tensile strength, increase resistance to water penetration, decrease contraction, reduce hairline and surface cracks, increase abrasive resistance, increase concrete resistance to vibration and stress, while reducing the need for a water-to-cement ratio.

Figure 4: Glass fibers

Steel Fibers

Steel fibers have different shape types, which can be straight or curved with varying dimensions [29]. To describe this parameter, a parameter called the aspect ratio is used. This parameter is calculated from dividing length by diameter (if the section is not circular, a circular dimeter equivalent to the intended section can be calculated). Also, these fibers are available in two hooked and simple states. This study used the hooked type of it, which could improve the quantity and quality of concrete properties.

Table 4: Steel fiber specifications

Name of fibers	Type of fibers	Length (mm)	Diameter (mm)	Aspect ratio	Tensile strength (MPa)
BSW-Fiber	Hooked	35	0.55	64	1100

The use of this type of fiber in concrete increases collapse strain, an increases resistance to impacts, energy absorption, stress and resistance to fatigue, resistance to thermal stresses and shrinkage, shear, flexural and compressive strength of concrete, and saves times, costs and materials, while increasing malleability or ductility.

Figure 5: Steel fibers

3.5. Instrumentation and loading systems

In the experiment, the lateral forces and drift of various areas of the wall were acquired by digital sensors and then recorded with an electronic data-processing device. Electronic drift-gauging devices were used to measure the drift of the areas of the sample under loading in different directions. Also, a static hydraulic jack, along with a controllable electrical pump, was used to apply the lateral force. Force was also measured by a dynamometer.
A hydraulic jack was also used to apply the gravity load to real-scale samples. Because the amounts of loads applied by the gravity-loading jacks change during the lateral loading, a special hydraulic jack was introduced, which was capable of balancing the gravity loading during the loading process. Also, a rolling system was devised to avoid the effects of the vertical jacks' application of gravity loads to the wall's in-plane motion when the lateral force was applied. This system was placed between the gravity load-applying jacks and the sample, which allowed the latter to easily move horizontally, while the sample was subject to the gravity load (Fig. 6).

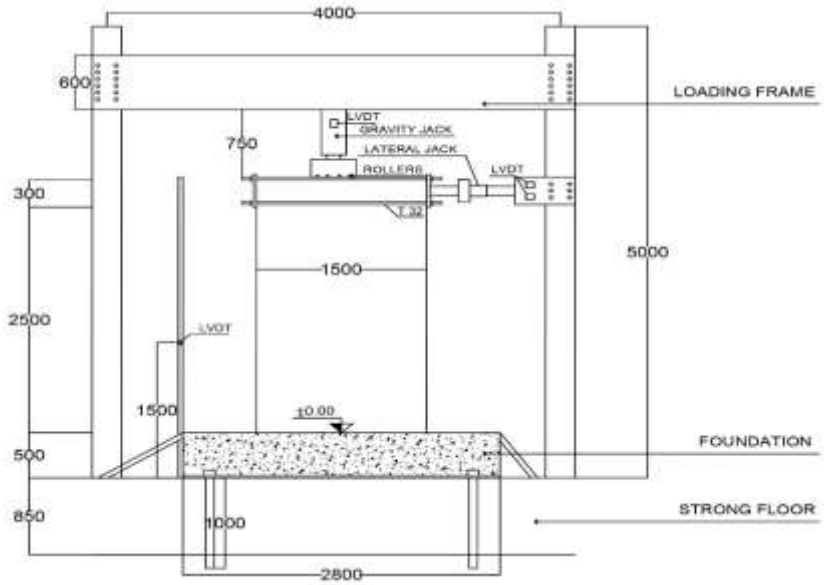

Figure 6: Schematic of the loaded sample

To record test data on the sample, instrumentation was applied. For this, three drift gauges were placed at different heights of the wall to record horizontal in-plane, diagonal and out-of-plane drifts. Another drift gauge was applied to control the sample's uplift and the foundation. Lateral forces were applied after the gravity load was applied. A data-recording device also recorded drift and force tests data. Reciprocal loading was performed based on AC-125 guidelines [30]. Consistent with this method and as indicated by Figure 7, the loading process is controlled by force prior to the cracking stage, while being controlled by drift after cracking. Prior to cracking, the forces applied will gradually increase by a certain amount. As the moment of cracking drift is revealed, the sample loading continues with the application of the enhance factor μ. Each stage of loading consists of a cycle in the force-controlled section and three complete cycles in the drift-controlled section. Notably, sample loadings were performed statically and at a low pace.

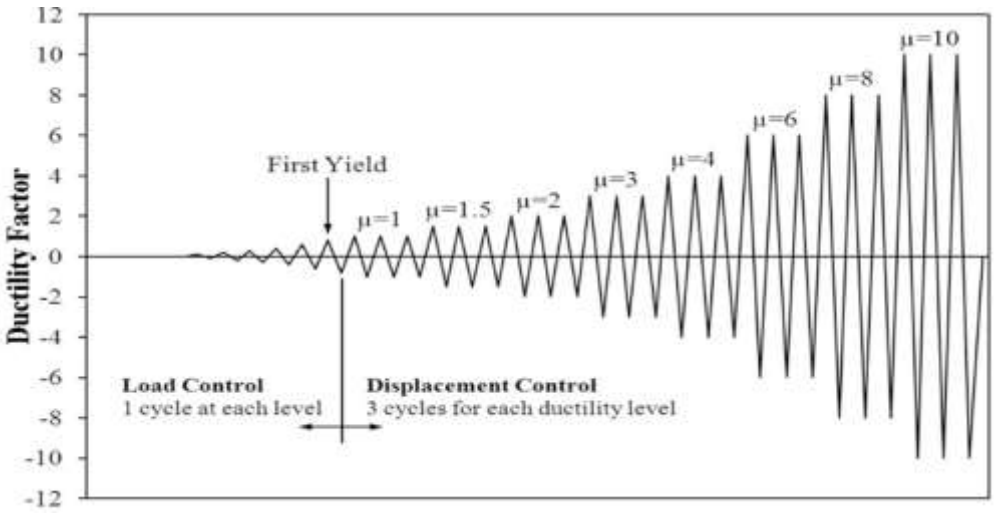

Figure 7: Loading pattern [30]

4. Test results

4.1. Observations

The UW walls

In the UW wall, cracking stared to occur within the two ends of the wall and in its two lower rows. The first visible cracks occurred at a relative drift of 0.1% and at a lateral load of 22 kN (50% of the ultimate strength) (Fig. 8).

Figure 8: UW wall

At a drift of 0.36% (a lateral load of 38 kN), shear cracks began to increase. Finally, after the full development of the cracks at a drift of 0.52% and at an ultimate load of 45 kN, the sample started to slip, which caused the cracking to develop. The failure mode of the sample was a rocking shear mode (Fig. 9).

Figure 9: Crack development at a drift

Figure 10 below illustrates the UW wall's hysteresis diagram

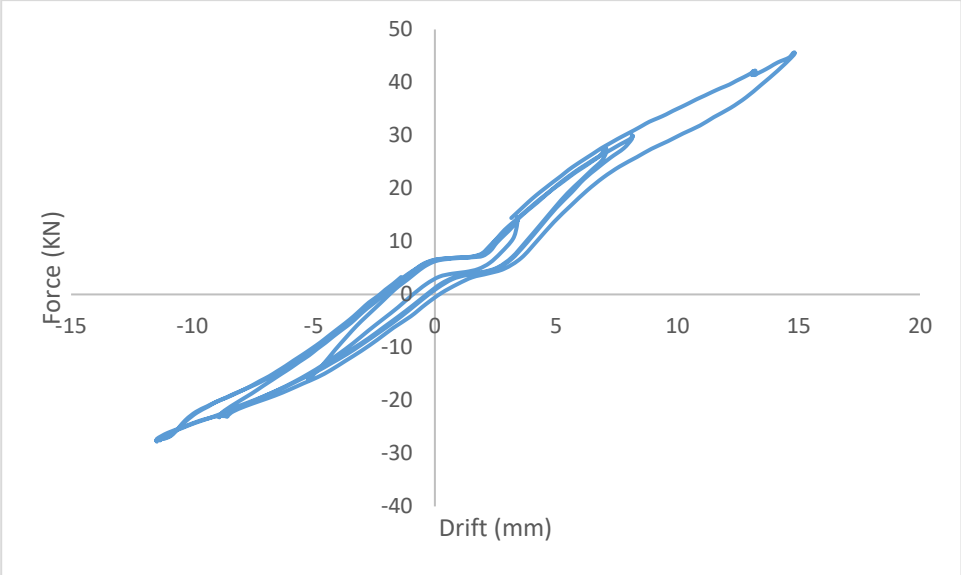

Figure 10: The UW wall's hysteresis diagram

RW1 wall

Cracking began to occur at the end of the wall and in the second row of it. The first crack appeared at a drift of 0.13% in both back and forth directions and at a lateral load of 25 kN (around 25% of the ultimate strength). As the test continued, this crack developed almost horizontally towards the other side of the sample, which resulted in the development of the second crack at a lateral load of 56 kN. Under this state, the sample began to slip and culminated in the development of the cracks.

Figure 11: RW_1 wall

In the end, the wall exhibited a resistance until an ultimate load of 106 kN and a drift of 1.98%. The rocking failure mode was found to be acceptable as it withstood the drift and the lateral force (Figures 11 and 12).

Figure 12: Development of cracks in the RW_1 wall

Figure 13 illustrates the hysteresis diagram of the RW_1 wall

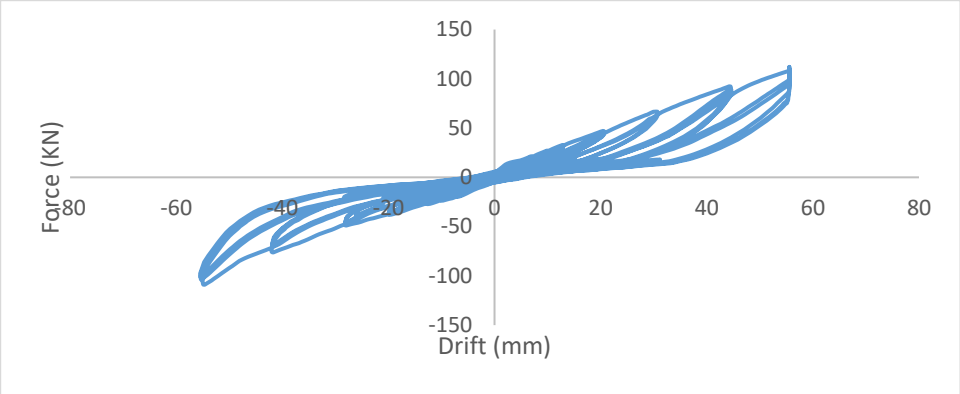

Figure 13: the hysteresis diagram of the RW_1 wall

RW_2 wall

In the RW_2 wall, cracking begins to appear at the end of the wall and in the first row of it. The first visible cracks occur at a drift of 0.57% and a lateral load of 52.5 kN (approximately 35% of the ultimate strength). As the test continued, the cracks developed at this sample place and moved toward the other side of the wall.

Figure 14: RW_2 wall

In the end, the wall began to crack at a drift of 2.28% and at an ultimate load of 150 kN. The failure model was rocking mode (Figure 15).

Figure 15: Development of cracks in the RW_2 wall

Figure 16 gives the hysteresis diagram of the RW_2 wall.

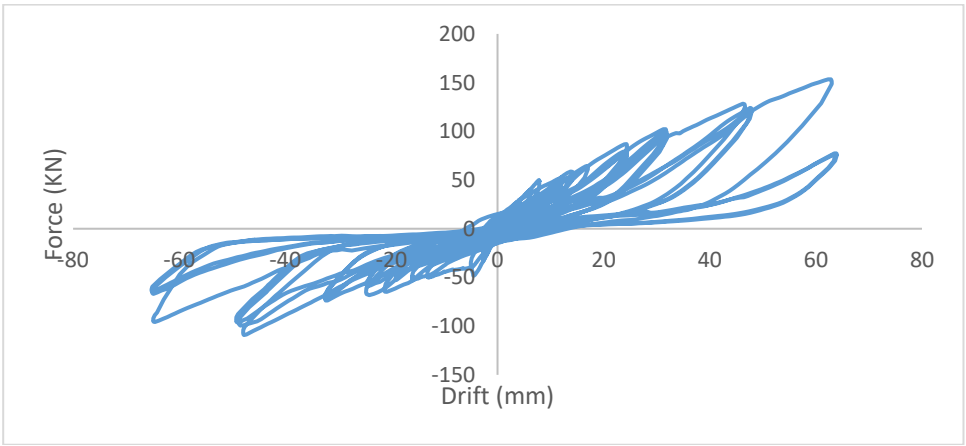

Figure 16: The hysteresis diagram of the RW_2 wall

Table 5 gives a summary of tests results. The control wall was subjected to loading to a drift of 0.52%, the RW_1 wall to a drift of 1.98%, and the RW_2 wall to a drift of 2.28%.

Table 5: Sample behaviors

Specimen	Limit States		
		Crack	resistance Maximum
Wall UW	Lateral Drift (%)	0.1	0.52
	Lateral strength (kn)	22	45
Wall RW_1	Lateral Drift (%)	0.13	1.98
	Lateral strength (kn)	25	106
Wall RW_2	Lateral Drift (%)	0.57	2.28

Lateral strength (kn)	52.5	153

4.2. Capacity (envelope) diagram analysis

Test results have been presented by an idealized force-drift diagram. Figure 17 illustrates that the capacity diagram (envelope curve) represents the connection of maximum resistances obtained from the first loading alternation at each specified drift [31].

UW, RW_1 and RW_2 samples held the highest resistances at 45, 106 and 150 kN, respectively. These values are close to the calculated values presented by Table 1. Therefore, equations based on standards, set for wall capacities, enjoy good accuracy. According to the results, the RW_1 wall experienced a maximum resistance of 2.1 times the UW wall's resistance, while the RW_2 saw a maximum resistance of 3.2 times the UW's wall and 1.5 times the RW_1 wall. Also, the UW, RW_1, and RW_2 walls respectively held greater deformation than the rest (Fig. 17).

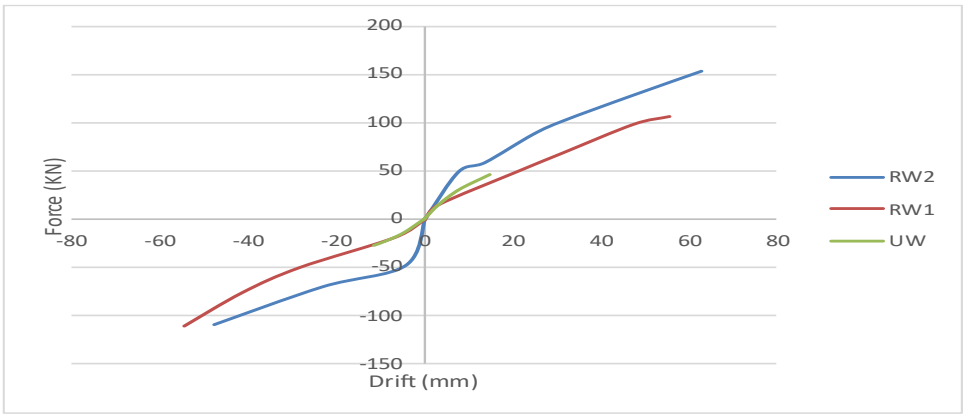

Figure 17: Comparing capacity (envelope curves) diagrams of the samples

In sum, retrofitted walls exhibited relatively ductile behaviors than the non-retrofitted wall. Notably, this ductility pertains to the in-plane shear slip failure mode. If this mode is incorporated into other modes such as out-of-plane failure modes (given the nature of seismic loads impacting in different directions), the sample will have a different behavior, which may aggravate its brittle behavior.

4.3. Energy dissipation

When the structure is subject to severe earthquakes, higher energy dissipation will be much useful and effective. The energy dissipated by a sample in an alternation is equal to the area under the hysteresis loop diagram of the sample's drift-force diagram in that alternation.

As illustrated by Figure 18, the hysteresis diagram of the samples was used to calculate the cumulative energy dissipation of the samples. The energy dissipated in the sample is dependent on the friction between the slits and cracks, the creation of new cracks and also brick crushing.

According to the results, the reinforced RW_1 and RW_2 samples respectively experienced much higher percentages of the non-plastic non-linear deformation capacity, while being capable of dissipating large amounts of energy compared to the unreinforced wall.

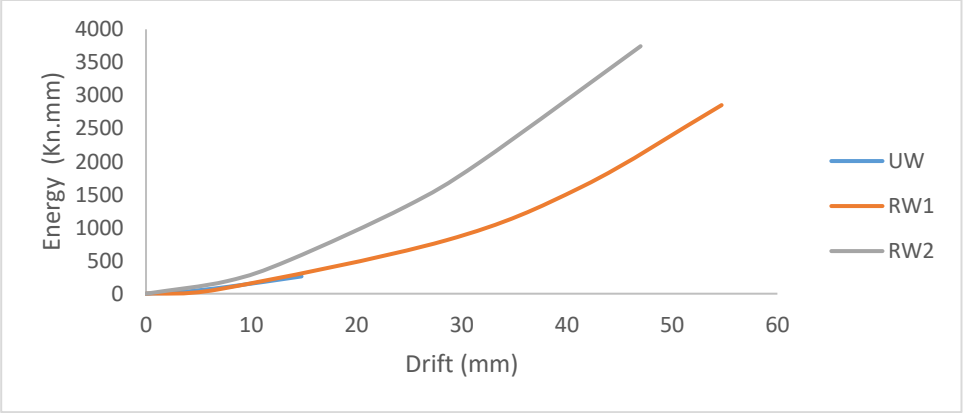

Figure 18: Cumulative dissipated energy of the samples

Figure 18 illustrates that the walls exhibited a considerable amount of energy absorption, after being reinforced by the hybrid fiber concrete. A one-side retrofitted wall exhibited around ten times and the two-side retrofitted wall exhibited twenty times energy dissipation than the unreinforced wall.

4.4. Drop in secant stiffness

Secant stiffness features a decline in resistances in the samples during the loading cycle. Secant stiffness in each alternation equals the linear slope that connects together the negative and positive maximums of the loads. Figure 19 illustrates the secant stiffness of the tested samples against inter-story drifts, showing that the RW_2 wall's stiffness is a bit higher than the RW_1 wall, and the RW_1 wall's stiffness is more than the UW wall.

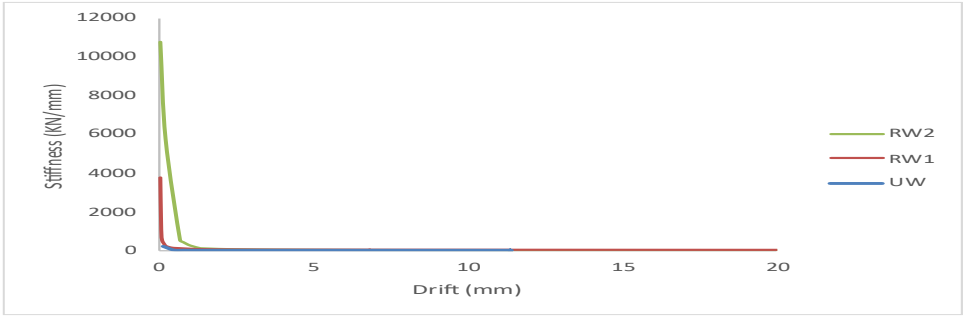

Figure 19: Declining secant stiffness of the samples

4.5. M factor analysis

According to ASCE-41 [32], the M factor characterizes structural component ductility, which is defined to be the same as the level of performance. This factor is determined by using an ideal drift-force diagram of test results. The first section of the ideal drift-force diagram begins from the center and has a slope equivalent to effective lateral stiffness. The lateral effective stiffness equals a secant stiffness of 60% of the structural yield strength, which cuts through the second section of the diagram to make the occupied levels on top of and bottom of the diagram be equal [33].

Figure 20 and Table 6 give the ASCE41-17-based ideal drift-force diagram, which is extracted from the average positive and negative sections of the drift-force diagram. The M factor for a specific performance level is calculated as a ratio of a drift at an intended performance level to a drift of a yield point on the idealized diagram.

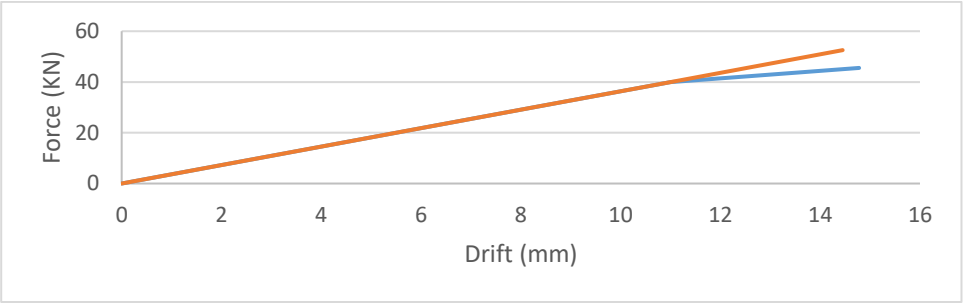

UW

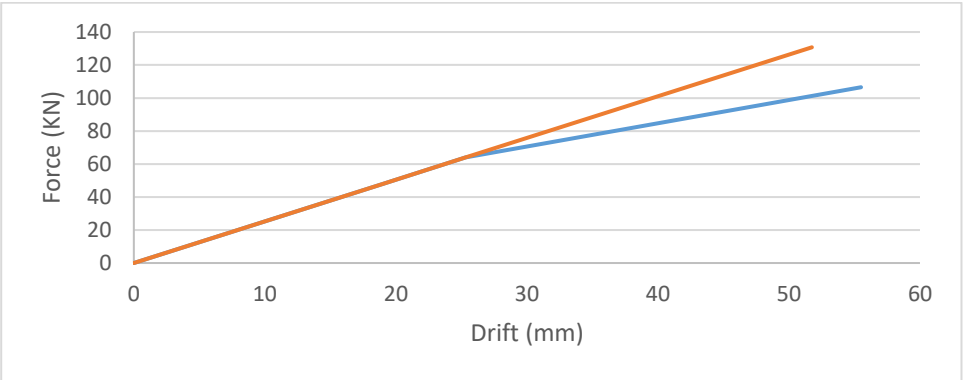

RW_1

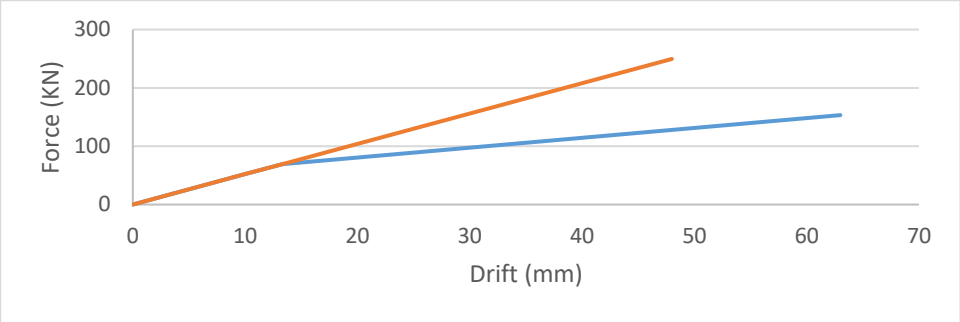

RW_2

Figure 20: Ideal drift-force diagrams based on ASCE 41-17

The M factor is considered for the drift of the Safety-Life (LS) Performance level, equivalent to 75% of the drift of the Collapse Prevention (CP) performance level and for the drift of Immediate Occupancy (IO), equivalent to 67% of the safety-life drift. Table 7 gives coefficients calculated for the tested samples.

Table 6: Various sections of the ideal drift-force diagram

Specimen	Lateral drift 1 (mm)	Lateral drift 2 (mm)	Lateral strength (KN)
Wall UW	11	14.78	45.5
Wall RW1	25.3	55.7	106.5
Wall RW2	13.3	64	153.3

The ASCE 41-17 Regulation was also added to the said table to compare the M factors introduced in Table 11-3. It is worth mentioning that according to regulation values, a confidence factor of 1.33 is considered, while no such a factor is considered for the M factors presented.
Results indicated that the M factors of the RW_2 wall are higher than those of the values suggested by the regulation. Also, the M factor of the reinforced walls was higher than that of the unreinforced wall, and the M factor of the two-side reinforced wall was also higher than that of the one-side reinforced wall.

Table 7: M factor for samples

Performance Level	ASCE 41-17	Specimens		
		Wall UW	Wall RW1	Wall RW2
IO	1	0.89	1.46	3.2
LS	3	1.33	2.1	4.8
CP	4	1.78	3	6.38

4.6. Behavior factor calculation

Designers seek to create safe and economic plans to reduce seismic impacts as much as possible, trying to avoid damages to the small and medium-sized structures, while maintaining their stability in large earthquakes. Many regulations have used a parameter called the behavior factor for reducing seismic force.
Experiments and calculations have produced different equations for calculating the behavior factor. This study used the University of Berkeley's practical findings [34] to calculate the behavior factor.

Equation (1)

$$R = R_s \; R_\mu \; R_R \; R_\xi$$

Where

R_s : Overstrength factor

R_μ : Factors arising from ductility

R_R : Undetermined coefficient

R_ξ : Damping coefficient

Determining R_s and R_μ values is a major goal of this study. According to Bertroud and Tiger's studies [35], the $R_\xi . R_R = 1$ and the R_ξ values can be considered equal to one for damping rates of 5%, as based on data provided by URC 194 [36].

The R_s value can be calculated from experimental and analytical methods such as non-linear static analyses, as in Equation 2 below:

Equation (2)

$$R_s = \frac{V_y}{V_d}$$

According to Equation (2), V_d represents the base shear force of the plan, as consistent with the Regulation, and V_y the yield shear force of the structure. In this study, V_d is equal to the shear force when the first plastic joint (V_s) is formed, and V_y is calculated from the bi-linearization of the shear curve by using the Priestley-Pauli method. The R_μ value is calculated from Equation (3):

Equation (3)

$$R_\mu = \frac{V_e}{V_y}$$

Where the V_e value is the shear force of the structural elastic deformation mode, which is calculated after the bi-linearization of the pushover curve using the above-stated method and making the area under the bi-linear diagram equal with the area under the structural elastic deformation diagram.

4.7. Method of bi-linearizing the pushover curve for calculating behavior factor parameters using the Priestley-Pauli method

This method was proposed by Priestley and Pauli [37] and was employed by the Applied Technology Council (ATC) [38]. Figure 21 below illustrates bi-linearization method using the Priestley-Pauli method.

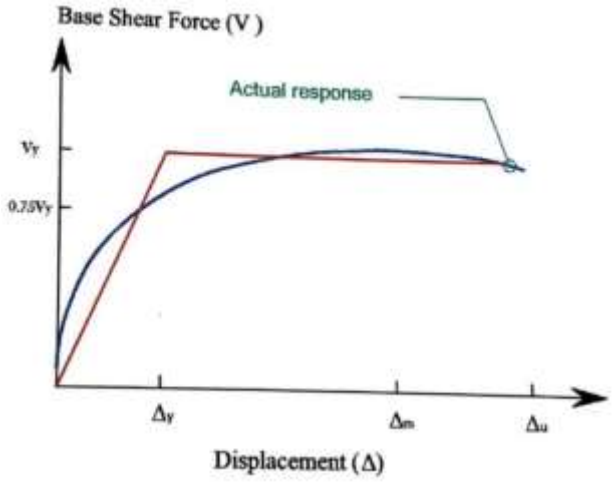

Figure 21: Bi-linearization using the Priestley-Pauli method

Required parameters for calculating R can be achieved by bi-linearizing the pushover curve and making the area under the bi-linear diagram equal to the area under the elastic diagram, as illustrated by Figure 21. Notably, this study considered maximum displacement of 60 mm for calculations, which was equal to the allowable deformation in the structural system.

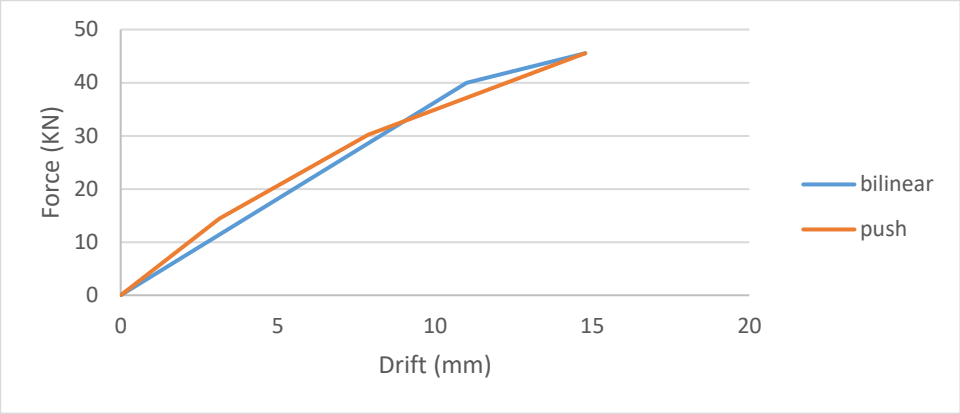

Figure 22: Bi-linear curve and the UW wall's elastic curve

According to experimental calculations, factors required for calculating R were determined and the R values were calculated (Figures 22, 23 and 24).

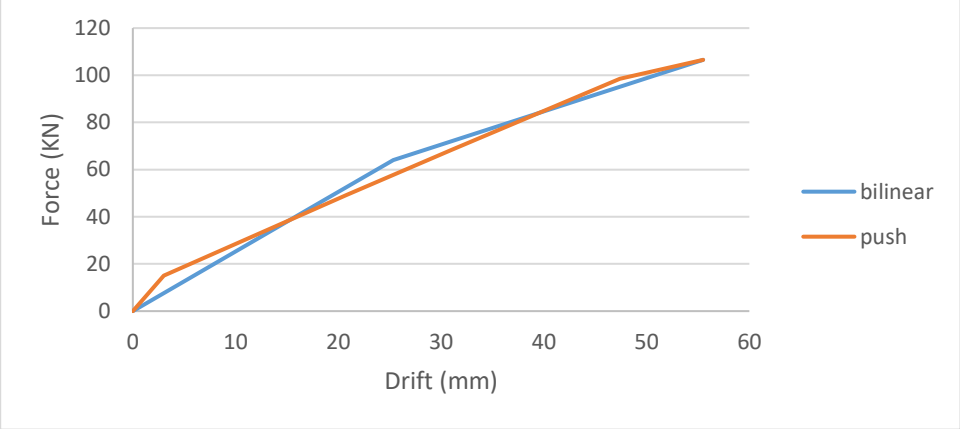

Figure 3: Bi-linear curve and the RW_1 wall's elastic curve

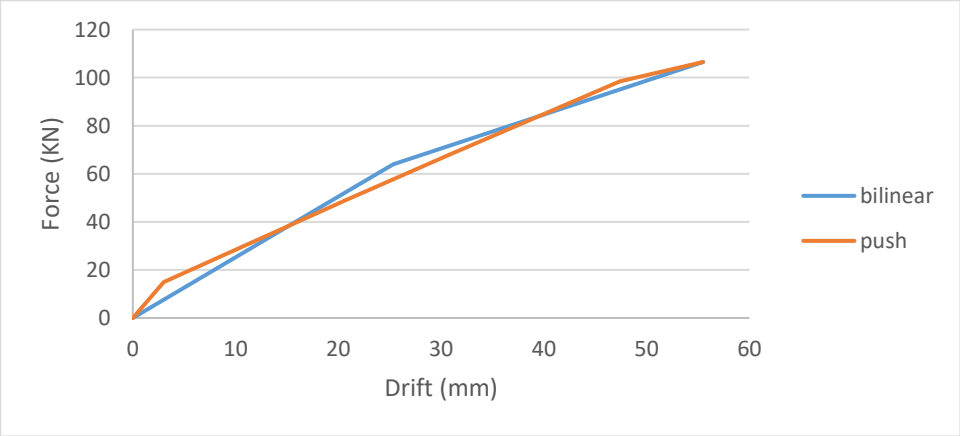

Figure 24: Bi-linear curve and the RW_2 wall's elastic curve

Table 8 below gives the calculation results.

Table 8: Calculating behavior factor parameters

Walls	$V_s\ (kN)$	$V_y\ (kN)$	$V_e\ (kN)$	R_μ	R_s	R
UW	22	40	52.5	1.31	1.81	2.37
RW_1	25	64	130.7	2.04	2.56	5.22
RW_2	34	69	249.6	3.62	2.02	7.3

Conclusion

This study presented reciprocal test results that investigated the in-plane behavior of masonry walls reinforced with hybrid fiber concrete. Experimental tests were carried out on three walls with fully identical geometries and on real scales. The study's main feature was the reinforcing of one side of a wall. Test results were as follows:

1. If reinforced well, masonry walls will be capable of maintaining a considerable percentage of their lateral strength even at low rates, after the occurrence of the first cracks. This results in a relatively ductile behavior in the wall and the involvement of other elements in the lateral load-bearing capacity of the masonry walls.
2. Using a hybrid fiber concrete face to retrofit masonry walls will significantly increase their stiffness and in-plane resistances.
3. According to the results, the maximum resistance of masonry walls reinforced with hybrid fiber concrete on two sides (RW_2) was around 1.4 times the resistance of masonry walls reinforced with hybrid fiber concrete on one side (RW_1), while being around 3.4 times that of the control wall (UW)
4. The RW_1 sample experienced a higher percentage of non-plastic non-linear deformation and was able to dissipate a large amount of energy compared to the unreinforced sample (UW). The total amount of energy dissipated in the one-sided reinforced wall (RW_1) was 16 times that of the unreinforced wall (UW).
5. Using the idealized drift-force diagram, the M factor, as a structural component ductility indicator, was calculated. This indicator indicates the level of performance and is compared to regulation values. The calculated values of the ductility coefficient in the reinforced wall (RW_1) saw an increase of about 2 times compared to the unreinforced wall (UW).
6. The samples' behavior factors were calculated by bi-linearizing the pushover curve. UW and RW_1 results were found to be 2.3 and 5.2, respectively, suggesting that the strengthening of masonry walls by using hybrid fiber concrete could leave a significant impact on enhancing the behavior factor, and thus reducing seismic force in structures.

References

[1] Russell, A. P., & Ingham, J. M. (2010, March). The influence of flanges on the in-plane seismic performance of URM walls in New Zealand buildings. In NZSEE Conference.

[2] Yaghoubifar, A. & Tasnimi, A.A. (2008). Experimental and Analytical Investigation of the Behavior of Strengthened Brick Walls by Steel Bars and Concrete. Master's Thesis, Tarbiat Modares University, Iran

[3] Abrams, D. P., & Shah, N. (1992). Cyclic load testing of unreinforced masonry walls. Illinois Univ at Urbana Advanced Construction Technology Center.

[4] Nateghi, F. & Alemi, F. (2008). Experimental study of seismic behavior of typical Iranian URH brick walls. The 14th World Conference on Earthquake Engineering, Beijing, China.

[5] Kadam, S. B., Singh, Y., & Li, B. (2014). Strengthening of unreinforced masonry using welded wire mesh and micro-concrete–Behaviour under in-plane action. Construction and Building Materials, 54, 247-257.

[6] Capozucca, R. (2011). Experimental analysis of historic masonry walls reinforced by CFRP under in-plane cyclic loading. Composite Structures, 94(1), 277-289.

[7] Yang, K. H., Joo, D. B., Sim, J. I., & Kang, J. H. (2012). In-plane seismic performance of unreinforced masonry walls strengthened with unbonded prestressed wire rope units. Engineering structures, 45, 449-459.

[8] Najif, I & Ingham, J. (2012). In-situ and laboratory based out-of-plane testing of unreinforced clay brick masonry walls strengthened using near surface mounted twisted steel bars. Construction and Building Materials. 36. 119-128. 10.1016/j.conbuildmat.2012.04.087.

[9] Applied Technology Council (ATC), Prestandard and Cemmentary for the seismic rehabilitation of buildings, publication No. 356, Federal Emergency Management Agency, Washington, D.C. (FEMA-356), 2000

[10] Naaman, . (2003). Engineered Steel Fibers with Optimal Properties for Reinforcement of Cement Composites. Journal of Advanced Concrete Technology. 1. 241-252. 10.3151/jact.1.241.

[11] G. Xu, S. Magnani, D.J. Hannant (1978), Durability of hybrid polypropylene-glass fibre cement corrugated sheets, Cement and Concrete Composites, 20(1), 79-84. https://doi.org/10.1016/S0958-9465(97)00075-9.

[12] Banthia, N., Moncef, A., Chokri, K. et al (1995). Uniaxial tensile response of microfibre reinforced cement composites. Materials and Structures **28**, 507–517. https://doi.org/10.1007/BF02473155

[13] Shah, S.P. (1991). Do fibers increase the tensile strength of cement-based matrices, ACI Materials Journal, RILEM 88(6), 595-602.

[14] Qian, C.X. & Stroeven, Piet. (2000). Development of hybrid polypropylene-steel fibre-reinforced concrete. Cement and Concrete Research. 30. 63-69. 10.1016/S0008-8846(99)00202-1.

[15] Dardaei, S., Shakib, H., Khalaf Rezaei, M., & Mousavi, M. (2014). Analytical and Experimental Seismic Evaluation of Confined Masonry Walls Retrofitted by Steel-Fiber and Polypropylene Shotcrete. Journal of Seismology and Earthquake Engineering, 16(4), 271-280.

[16] Najafgholipour, M.A & Dehghan, S. M. & Mirzaee, A.et al. (2016). Experimental Investigation on Flexural Behavior of Masonry Prisms Strengthened by Fiber-Reinforced Mortar Layer. Iranian Journal of Science and Technology, Transactions of Civil Engineering. 40. 10.1007/s40996-016-0035-y.

[17] Khajepour, M. (2015). Experimental investigation of fiver concrete coating on the in-plane behavior of unreinforced brick walls; M.S. Thesis, University of Technology, Shiraz, Iran

[18] Kamrava, A.; Najafgholipour, M.A.; Dehghan, S.; & Khajepour, M.; (2016). Numericla investigation of the in-plane behavior of unreinforced masonry walls retrofitted with fiber concrete, 9th National Congress on Civil Engineering, Mashhad, Iran

[19] Najafgholipour-Haghighi, M. A.; Y.M. Ziaei, & Karamian, R. (2019). Experimental investigation of the in-plane behavior of unreinforced masonry panels retrofitted with steel fiber concrete faces, 11th National Congress on Civil Engineering, University of Shiraz, Iran.

[20] Yugandhar, B. & Krishna, B. & Bharath, B. & Chandra, J. & Reddy, M.N. (2017). Experimental study and strength of concrete by using glass and steel fibres. International Research Journal of Engineering and Technology (JRJET), 4(12), 1108-1116.

[21]Vikrant S. Vairagade, Shrikrishna A. Dhale. (2023). Impact resistance of hybrid steel fiber reinforced concrete, Hybrid Advances, Volume 3, 2023, 100048.

[22] Guoan Liu, Xin Wang, Jian Zhu, Zhe Yang, Hao Chen, Nan Wu, Yuanhao Liu, Shaowei Hu. (2023). Effects of aspect ratios and strengthening methods on seismic behavior of masonry piers strengthened by using hybrid-fibers modified reactive powder concrete,

Journal of Building Engineering, Volume 77, 107385.

[23]Seyed Rahman Seyed Rezaee, Masoud Soltani, Morteza Nikooravesh. (2022). Cyclic in-plane behavior of unreinforced and confined masonry walls retrofitted by shotcrete: Experimental investigation, Engineering Structures,Volume 264, 2022, 114432.

[24]Babar Ali, Liaqat Ali Qureshi, Rawaz Kurda. (2020). Environmental and economic benefits of steel, glass, and polypropylene fiber reinforced cement composite application in jointed plain concrete pavement, Composites Communications, Volume 22, 2020, 100437

[25] ASCE 41-17 (2017). Seismic evaluation and retrofit of existing buildings. American Society of Civil Engineers (ASCE).

[26] Code No. 360 (2013). Instruction for seismic rehabilitation of existing buildings. Management and Planning Organization (Deputy for Technical Affairs). In Persian.

[27] Mazroui, A. & Yaghoubifar, A. & Ardakani, M.H.M. & Nejad, E.Z. & Jafarpour, F. (20120). Experimental evaluation of mechanical properties of conventional sand-cement mortars (for brick work). Building & Housing Research Center, Tehran, Iran. In Persian.

[28] Yugandhar, B. & Krishna, B. & Bharath, B. & Chandra, J. & Reddy, M.N. (2017). Experimental study and strength of concrete by using glass and steel fibres. International Research Journal of Engineering and Technology (JRJET), 4(12), 1108-1116.

[29] American Society of Civil Engineers (2006). Seismic Rehabilitation of Existing Buildings, ASCE 41-06, Reston, Virginia.

[30] AC 125. (2010). Acceptance Criteria for concrete and reinforced and unreinforced masonry strengthening using externally bonded fiber-reinforced polymer (FRP) composite systems. ICC Evaluation Service.

[31] ASCE 41-130 (2013). Seismic evaluation and retrofit of existing buildings. American Society of Civil Engineers.

[32] ASCE 41-17 (2017). Seismic evaluation and retrofit of existing buildings. American Society of Civil Engineers.

[33] Naaman, A. (2003). Engineered Steel Fibers with Optimal Properties for Reinforcement of Cement Composites. Journal of Advanced Concrete Technology. 1. 241-252. 10.3151/jact.1.241.

[34] Structural response modification factor (1995). Applied Technology Council No. 19.

[35] Whittaker, A. & Uang, C-M. & Bertero, V. (1987). Earthquake simulation tests and associated studies of a 0.3 scale model of a six story eccentrically braced steel structure. 10.13140/RG.2.1.2503.8964

[36] O. International Conference of Buildings, Uniform Building Code, International Conference of Building Officials, Whittier, Calif, 1994.

[37] Paulay, T. & Priestley, M.N. (1992). Seismic design of reinforced concrete and masonry buildings.

[38] ATC (1995). Structural response modification factors, ATC-19 report, Applied Technology Council, Redwood City, California.